



Asymmetrical Deformation Mechanisms in Layered Inclined Surrounding Rock of Roadways



Lei Tan^{1,2}, Xuan Zhan^{1,2}, Hu Zhen^{1,2}, Jiaren Chen^{1,2}, Hai Wu^{1,2*}

¹ School of Resources, Environment and Safety Engineering, Hunan University of Science and Technology, 411201 Xiangtan, China

² Work Safety Key Lab on Prevention and Control of Gas and Roof Disasters for Southern Coal Mines, Hunan University of Science and Technology, 411201 Xiangtan, China

* Correspondence: Hai Wu (wuhai@hnust.edu.cn)

Received: 11-14-2023

Revised: 12-15-2023

Accepted: 12-21-2023

Citation: L. Tai, X. Zhang, H. Zhen, J. R. Chen, and H. Wu, "Asymmetrical deformation mechanisms in layered inclined surrounding rock of roadways," *GeoStruct. Innov.*, vol. 1, no. 1, pp. 17–31, 2023. <https://doi.org/10.56578/gsi010102>.



© 2023 by the authors. Published by Acadlore Publishing Services Limited, Hong Kong. This article is available for free download and can be reused and cited, provided that the original published version is credited, under the CC BY 4.0 license.

Abstract: In the context of layered inclined surrounding rock in roadways, this study presents a comprehensive analysis focusing on the asymmetrical deformation characteristics inherent to such geological structures. The intersection of layered surrounding rock with roadways forms the basis for constructing a deformation partition model, encompassing distinct sub-regions around the roadway. This model facilitates a detailed mechanical analysis, wherein the stress exerted on rock formations within each sub-region is meticulously examined. Consequently, specific mechanical formulas correlating to the stress in different sub-regions are established. This approach yields insights into the failure modes of the layered surrounding rock across various sub-regions. Notably, the roadway's high side predominantly exhibits tensile failure, whereas the low side is characterized by shear failure. The application of the Goodman model enables a simulation of interlayer slip occurring between the surrounding rock of the roadway, distributed across different partitions. This study delineates the deformation of the layered inclined surrounding rock roadway as a process with pronounced temporal characteristics. The progression of deformation and failure in the surrounding rock typically initiates at the tangent point between the roadway roof and the rock layer, extending to the roadway floor, the high-top bottom angle, and subsequently the low-top bottom angle. This sequence culminates in the development toward the high-top shoulder angle. The research further establishes a direct correlation between the onset of asymmetrical deformation and the angle of shear stress on the roadway surface relative to the inclination of the rock formation; a smaller angle precipitates an earlier onset of this deformation.

Keywords: Inclined strata; Unsymmetrical deformation; Surrounding rock; Deformation zone

1 Introduction

Coal is the foundation of world economic and social development. It has been second only to oil for a long time, accounting for 27.2% of the important energy in the global energy consumption structure. In 2021, coal will already account for 56% of China's energy consumption structure comparison. China is also the largest country in coal production. In 2021, the global coal output will be 7.889 billion tons, and China's coal output will be 4.071 billion tons. China's coal mining directly has a significant impact on the world's coal production and consumption patterns. With the gradual exhaustion of shallow resources, deep coal mining is an inevitable trend of coal mining [1, 2]. The occurrence of coal in China determines that China's coal mines are mainly underground mining, and many tunnels need to be dug underground. According to incomplete statistics, the total length of newly excavated roadways in China's coal mines is nearly 20,000 kilometers every year. Keeping the roadways smooth and maintaining the stability of the roadways is of great significance to the construction and production of coal mines. Statistics show that about 55% of China's recoverable coal reserves are found in sloping rock formations. Among the 50 counted kilometer deep mine, there are 38 mines whose inclination angle is greater than 10°, and 11 of which have rock formations whose inclination angle exceeds 30° [3]. Field measurements show that the inclination of rock formations increases the complexity of roadway support. When the inclination angle of rock formation is more than 10°, it has obvious influence on the deformation of deep roadway. The deformation of the surrounding rock of the roadway

shows asymmetric characteristics such as time non-uniformity and spatial asymmetry. Especially after entering the deep mining, the deep nonlinear mechanical system [4] and surrounding rock stability are related to the dip angle of the coal seam, the length of the shear plane and the physical and mechanical parameters of the coal and rock mass [5]. Zhou et al. [6] established the instability model of the upper coal mass by using the Bishop algorithm, and deduced the calculation formula of the stability safety factor of the upper coal mass. Scholars have established a mechanical model for the stability of the roof “triangular structure” by establishing a mechanical model [7–9] and a plastic zone mechanical model [10, 11] based on the two coal bodies in the mining roadway under the action of bearing pressure [12–14]. Using elastic-plastic mechanics and the theory of rock pressure to reveal the law of rock pressure in steeply inclined coal seam roadways [15–18], and put forward the calculation formula of entropy flow of roadway roof support system [19–21]. It is concluded that the deformation and failure characteristics of the surrounding rock in the steeply inclined coal seam roadway are different in the range of the loose circle and the uneven stress distribution of the surrounding rock [22]. The lateral and vertical deformation and evolution characteristics of the two sides and roof of the dynamic pressure roadway at different depths were quantitatively analyzed [23]. Using the theory of slip line field, the slip line field of shear-slip failure of homogeneous elastic-plastic surrounding rock and the calculation formula of ultimate load including failure characteristic parameters are obtained [24]. It is confirmed that the lithology of the surrounding rock and the size of the roadway section are important factors affecting the fracture range of the surrounding rock [25]. The mechanism and influencing factors of four types of kick drums, including squeeze-fluid kick drum, flexurally folded kick drum, shear dislocation kick drum and water-expandable kick drum, were analyzed [26]. On the basis of theoretical analysis, a support design scheme was proposed [27], and an integral closed support was constructed with active supports such as bolts, anchor cables and grouting as the main body [12, 13, 28, 29]. The anchor-net-cable coupling support design scheme is proposed in a targeted manner [30]. These researches have a certain guiding role for the formulation of support schemes for shallow steeply inclined and deep high-stress roadways, but it is necessary to do further research on the influence of inclination angle on roadway deformation. Li et al. [31] studied the evolution law of the distribution characteristics of the butterfly-shaped plastic zone of the roadway with the deflection of the principal stress direction of the surrounding rock, and revealed the formation mechanism of the butterfly leaf directionality of the butterfly-shaped plastic zone of the roadway. Through big data analysis, Meng et al. [32] studied the law of rock inclination α , the angle between the rock strike and the tunnel axis β , the maximum principal stress of the original rock stress field and the angle between the rock layer, and asymmetric deformation. Liu and Zhang [33] believed that the mechanical properties of layered rock mass change due to the change of the angle between the layer and the principal stress. Li et al. [34] believed that the greater the inclination angle of the rock formation, the greater the probability of the failure of the tunnel to slide along the bed, and the surface subsidence, vault displacement, and principal stress of the surrounding rock increase with the increase of the inclination angle. Hu [35] believed that the strength of layered rock showed a U-shaped distribution law with the increase of the layer angle, and the degree of anisotropy of the layered rock decreased with the increase of the confining pressure. Tian et al. [36] studied the non-uniform deformation characteristics of tunnels. Wu et al. [37], Wu et al. [38], and Jia et al. [39] studied the non-uniform deformation with good layering through similar simulation experiments. Li et al. [40] and Wu et al. [41] think that the influence of confining pressure on Young's modulus is very significant. Zhang et al. [42] investigated the difference between uniform radial and non-uniform convergence deformation patterns on the surface settlements and lateral deformation of soil. All of these analyses have done some research on the deformation characteristics and deformation mechanism of the layered inclined surrounding rock roadway, but the research on the mechanism of non-uniform deformation in different parts of the roadway surrounding rock is not clear enough.

2 Study on Deformation Characteristics of Deep Inclined Rock Strata Roadway Subareas

The deformation and failure process of the deep inclined roadway is affected by the layered joints and the inclination angle of the rock formation, thus showing different characteristics from the ordinary near-horizontal roadway. Combined with the rock mechanical parameters, occurrence conditions and deformation and failure characteristics of the surrounding rock of the deep inclined roadway, and using the relevant theories of material mechanics and rock mechanics [43, 44], the surrounding rock of the deep layered inclined roadway is divided according to the deformation and failure characteristics of the surrounding rock.

2.1 Deformation Properties Measurement and Analyses of Inclined Rock Strata Roadway

The elevation of the roadway floor of Qujiang Mine is -850 m, the surface elevation is 40-50 m, and the dip angle of the rock formation is 15°. The surrounding rock of the roadway shows asymmetric deformation characteristics: the roadway floor is asymmetrically deformed, the deformation of the high side is large, and the deformation of the low side is small. The deformation characteristics of the high and low sides of the roadway are different. The shoulder angle of the low side is severely deformed, while the high side is relatively stable. As shown in Figure 1.

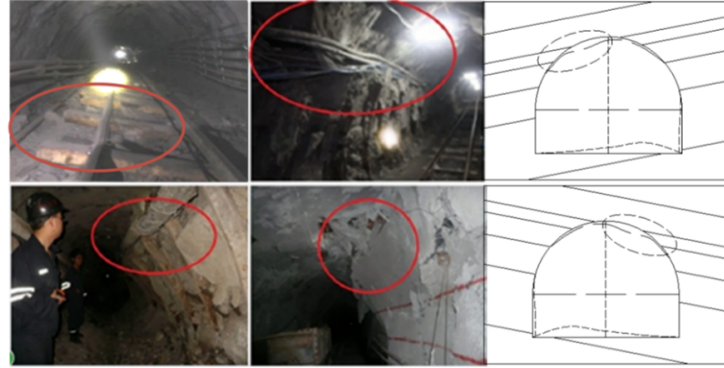


Figure 1. Asymmetric deformation distribution of roadway surrounding rock

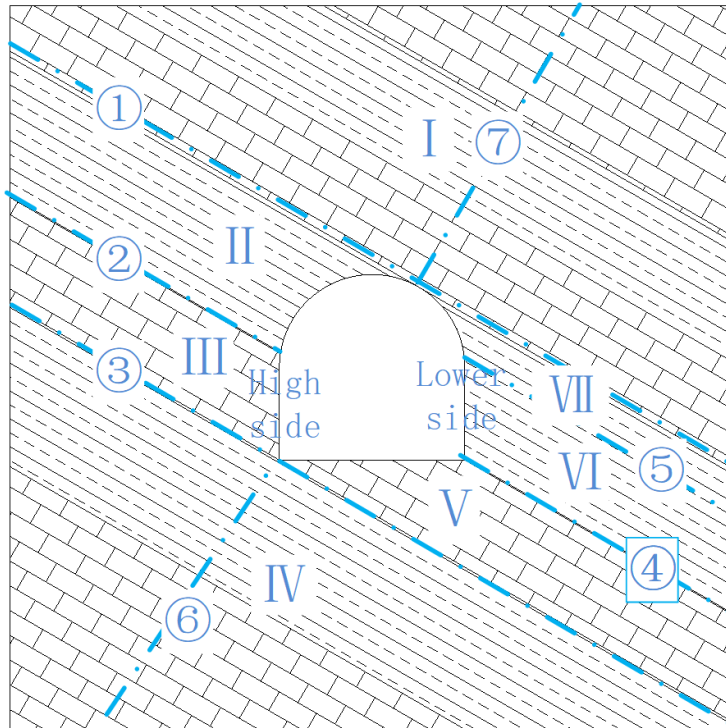


Figure 2. Deforming destruction zone division of roadway inclined rock strata

2.2 Deformation Subareas of Layered Inclined Surrounding Rock of Roadway

Generally, the horizontal or near-horizontal layered surrounding rock of the roadway is divided into four areas and three parts for research, which are the roadway roof, bottom plate and both sides of the roadway [45]. However, due to the existence of rock inclination, the partition of deep inclined rock roadway still cannot describe the roadway deformation effectively by using this method. Therefore, the surrounding rock of the deep layered inclined roadway is divided into more detailed deformation areas, and the surrounding rock failure of the roadway is divided into 7 different areas according to the positional relationship between the layered surrounding rock and the roadway and the deformation difference of the roadway surrounding rock, as shown in Figure 2.

In Figure 2, the four partition lines (dotted lines ①, ②, ③, and ④) are parallel to the inclination of the rock formation. After the four partition lines intersect the surface of the roadway, the surrounding rock of the roadway is divided into 7 areas. The ① subdivision line is tangent to the roof of the roadway, and the area above this line is divided into Zone I; The ③ subdivision line intersects with the bottom corner of the roadway, and the area below this line is divided into Section IV; The high gang and the adjacent roof area included in the middle of the two partition lines of ① and ③ are divided into Zone II and Zone III by the ② partition line passing through the intersection of the surface line of the high gang and the roof; The low-top and the adjacent bottom plate area included in the middle of the two partition lines of ① and ③ are divided into V and VI areas by the ④ partition line passing through the intersection of the low-top surface line and the bottom surface line. Partition line No. ⑤ divides the surrounding

rock at the shoulder angle of the low-top-side and the roof into Zone VI and Zone VII from the tangent position of the roof and the low-top. The integrity of the rock formation in Zones I and IV was not damaged by roadway excavation, while the rock masses in Zones II, III, V, VI and VII were damaged by roadway excavation. Therefore, according to the constraints and failure forms of rock mass in different regions, mechanical models are established respectively, and simplified mechanical analysis is carried out [46, 47].

2.3 Mechanics Analysis of Different Rock Deformation Subareas

According to the surrounding rock structural conditions, mechanical conditions and deformation mechanism of different partitions, the structural models of surrounding rock deformation and failure of deep layered inclined roadways can be divided into two categories according to the integrity of the rock stratum: the rock stratum is intact and the rock stratum is cut off by the roadway. The rock mass in Zone I and Zone IV in Figure 2 belongs to the rock formation integrity type; Zone II, Zone III, Zone V, Zone VI and Zone VII belong to the cut-off type of roadway.

(1) Mechanical model of rock mass deformation in zone I and zone IV

The integrity of the layered surrounding rock in Zone I and Zone IV is not affected by the roadway excavation, and the bending deformation of the surrounding rock in Zone I is symmetrically distributed on the normal line ⑦ of the tangent point between the rock layer and the roof of the roadway; The bending deformation of the surrounding rock in the IV area is symmetrically distributed with the normal line of the rock stratum high, the upper and the bottom angle ⑥, and the mechanical model of the deformation of the rock mass beam is established. The rock inclination angle is α , the axial load of the rock mass beam is F , and the normal uniform load concentration is $q_1(x)$, and the resistance load concentration of adjacent rock mass beams is $q_2(x)$. The length of the rock mass beam is L (the influence range of the roadway deformation and the length of the intersection of the rock formation), as shown in Figure 3.

Therefore, the bending moment equation of the rock mass beam is:

$$M(x) = \frac{qL}{2}x - \frac{q}{2}x^2 - Fw \quad (1)$$

Among them, F is the bedding pressure on both ends of the rock mass beam; $q = q_1(x) - q_2(x)$; w is the deflection line of the rock mass beam. If the bedding pressure on both ends of the rock mass beam is not considered, that is: $F = 0$, then there are:

$$M(x) = \frac{qL}{2}x - \frac{q}{2}x^2 \quad (2)$$

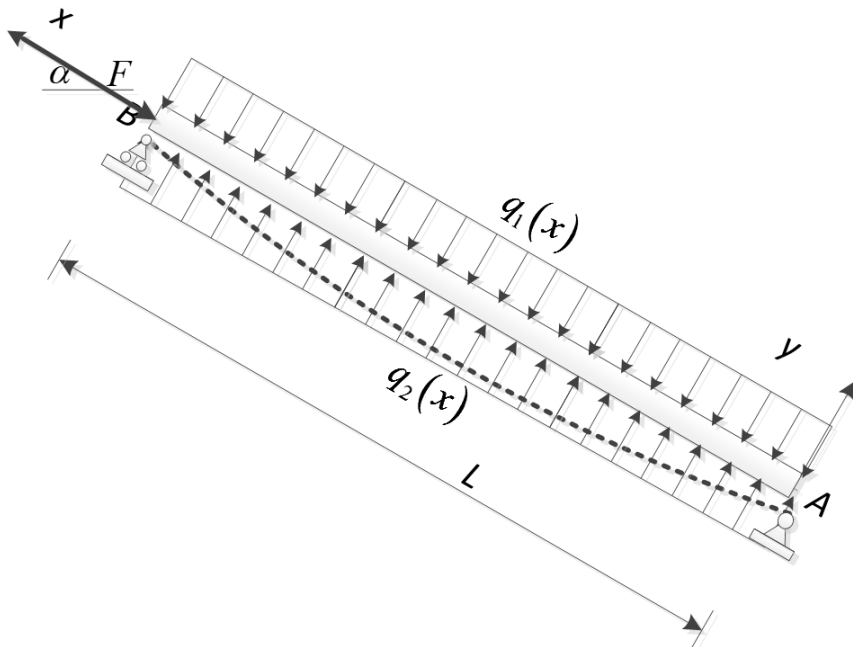


Figure 3. Mechanical model of bending deformation of complete rock mass beam

There is a maximum value for $M(x)$ when $x = \frac{L}{2}$:

$$M(x)_{\max} = \frac{qL^2}{8} = \frac{[q_1(x) - q_2(x)] L^2}{8} \quad (3)$$

2.4 Mechanical Model of Rock Mass Deformation in Zone II and Zone III

The lower part of the rock formation in Zone II and Zone III intersects with the roadway, the inclination angle of the rock formation is α , and the uniform load of the inclined rock mass beam is $q_1(x)$. The resistance load of the adjacent rock beam is $q_2(x)$. The length of the inclined rock mass beam is l . As shown in Figure 4.

The deformation of the surrounding rock mass of the roadway can be obtained according to the deflection equation of the structural rock mass beam. According to the superposition method of deflection deformation, the deflection equations of $q_1(x)$ and $q_2(x)$ are obtained respectively, and then superimposed. The deflection equations for $q_1(x)$ and $q_2(x)$ are:

$$w_1 = \frac{-q_1(x)}{24EI} (x^2 - 4lx + 6l^2) \quad (4)$$

$$w_2 = \frac{-q_2(x)}{24EI} (x^2 - 4lx + 6l^2) \quad (5)$$

The bending moment equation of the rock mass beam can be obtained as:

$$M(x) = \frac{-[q_1(x) - q_2(x)] (l - x)^2}{2} \quad (6)$$

2.5 Mechanical Model of Rock Mass Deformation in Zone V, zone VI and Zone VII

Similarly, see Figure 5, the deformation of the rock formation in the V, VI and VII areas can be calculated according to the deflection equation of the rock beam. The deflection equation of the rock layer can be calculated according to the superposition method of deflection deformation, and the deflection equations of $q_1(x)$ and $q_2(x)$ can be obtained respectively, and then superimposed. The deflection equations that can have $q_1(x)$ and $q_2(x)$ are:

$$w_1 = \frac{-q_1(x)}{24EI} (x^2 - 4lx + 6l^2) \quad (7)$$

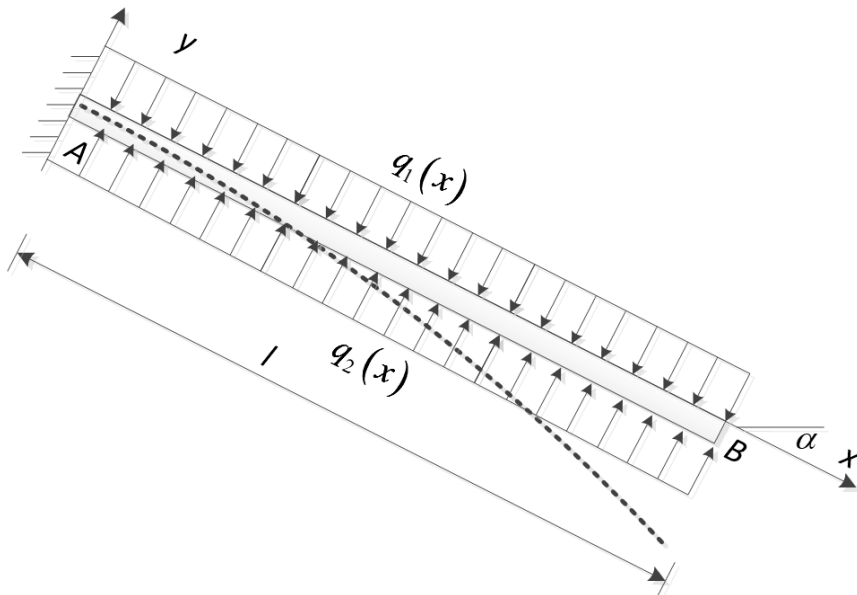


Figure 4. Mechanical model of bending deformation of rock mass beam

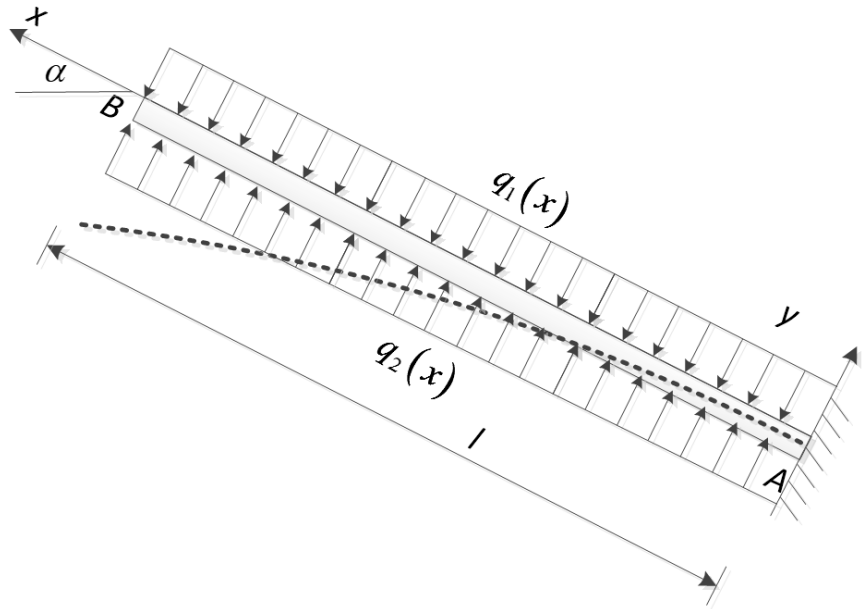


Figure 5. Bending deformation mechanical model of rock mass beam

$$w_2 = \frac{-q_2(x)}{24EI} (x^2 - 4lx + 6l^2) \quad (8)$$

From this, the bending moment equation of the rock mass beam can be obtained as:

$$M(x) = \frac{-[q_1(x) - q_2(x)](l-x)^2}{2} \quad (9)$$

2.6 Criteria for Surrounding Rock Failure of Layered Inclined Roadway

The failure of the surrounding rock of the layered inclined roadway is the shear failure or tensile failure of the surrounding rock under stress and strain conditions, that is, the shear force or tensile force of the surrounding rock of the roadway exceeds the shear strength or tensile strength.

$$\sigma_c \geq [\sigma_c] \text{ or } \tau_T \geq [\tau_T]$$

In the formula, σ_c is the tensile stress in the rock mass beam, $[\sigma_c]$ is the tensile strength of the rock material; τ_T is the shear stress in the rock mass beam, and $[\tau_T]$ is the shear strength of the rock material.

2.7 Tensile Failure Criterion of Surrounding Rock in Layered Inclined Roadway

The tensile stress on the cross-section of the rock mass beam in different partitions of the surrounding rock of the layered inclined roadway is the criterion for judging whether the rock mass beam has tensile failure, as shown in Figure 6.

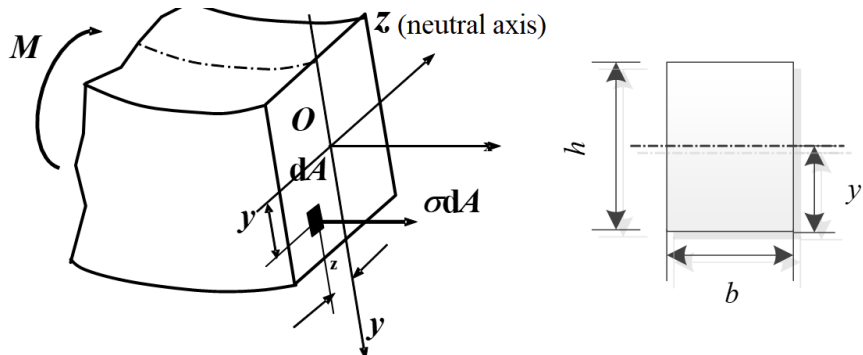


Figure 6. Mechanical relationship diagram of rock mass beam

The tensile stress in the rock mass beam is:

$$\sigma_c = \frac{My}{I} \quad (10)$$

where, M is the bending moment in the section of the rock mass beam; y is the distance between the neutral axis of the rock mass beam and the surface of the rock mass beam, the unit is m ; I is the moment of inertia of the rock mass beam section about the neutral axis. The structural section of the rock mass beam is a rectangular section, so there are:

$$I = \frac{bh^3}{12}, y = \frac{h}{2} \quad (11)$$

where, b is the width of the rock mass beam, m ; h is the thickness of the rock mass beam, the unit is m . Substituting 11 into 10 gives:

$$\sigma_c = \frac{My}{I} = \frac{M(h/2)}{bh^3/12} = \frac{6M}{bh^2} \quad (12)$$

According to the beam bending theory of material mechanics, the maximum bending moment equations of structural rock mass beams in zone I and zone IV are as follows:

$$M(x)_{\max} = \frac{[q_1(x) - q_2(x)] L^2}{8} \quad (13)$$

Therefore, the maximum stress expression of the rock mass beam in Zone I and Zone IV is:

$$\sigma_{c\max} = \frac{3[q_1(x) - q_2(x)] L^2}{4bh^2} \quad (14)$$

Because the maximum bending moment equation of the rock mass beam in the II area, III area, V area, VI area and VII area is:

$$M_{\max} = \frac{[q_1(x) - q_2(x)] l^2}{2} \quad (15)$$

The maximum stress expressions of rock mass beams in Zone II, Zone III, Zone V, Zone VI and Zone VII are obtained as:

$$\sigma_{c\max} = \frac{3[q_1(x) - q_2(x)] l^2}{bh^2} \quad (16)$$

If: $\zeta = \frac{[q_1(x) - q_2(x)]}{bh^2}$.

From this there are:

The maximum stress expressions of rock mass beams in Zones I and IV are:

$$\sigma_{c\max} = \zeta \frac{3L^2}{4} \quad (17)$$

The maximum stress expression of the rock mass beam in the II zone, III zone, V zone, VI zone and VII zone is as follows:

$$\sigma_{c\max} = \zeta 3l^2 \quad (18)$$

The tensile failure criterion of rock mass beam is:

$$\sigma_{c\max} \geq [\sigma_c] \quad (19)$$

It can be seen from this that the length L of the rock mass beam is related to l . The longer its length is, the easier the bending internal force in the rock mass beam is to exceed its ultimate tensile strength, resulting in tensile failure of the rock mass beam.

Further analysis in combination with Figure 2 shows that the length of the rock mass beam is longer in the junction area of Zone I, Zone II and Zone VII and the junction zone of Zone IV, Zone III and Zone VII, so the tensile failure occurs first in these two areas. However, the length of the rock mass beam is relatively short in the junction area of II and III and in the junction of V and VI and VII, so the tensile failure occurs relatively late in these areas.

2.8 Analysis of Stress Direction in Surrounding Rock of Layered Inclined Roadway

After the excavation of the roadway, the original rock stress field of the surrounding rock of the roadway was destroyed, and the rock mass on the roadway surface changed from the original three-direction force to the two-direction force, as shown in Figure 7.

The inclination angle of the rock formation in the surrounding rock of the layered inclined roadway is α , and the horizontal stress is σ_h and the vertical stress is σ_v in the area around the roadway that is not affected by the roadway excavation. Due to the formation of free face of the rock mass near the surface of the roadway, the directions of these two forces change, and are converted into a force σ_t tangential to the surface of the roadway and a force σ_r perpendicular to the surface of the roadway.

(1) Stress Analysis of Rock Mass in Areas II and VII

Due to the excavation of the roadway, the integrity of the rock formations in Zones II and VII is damaged, which also affects the stress characteristics of the rock mass in the zones. Figure 8 is a schematic diagram of the force of the rock mass on the roadway surface in Zone II. Due to the excavation of the roadway, the normal stress rotation of the roadway surface is parallel to the roadway surface, so on the roadway surface, the stress σ_r is zero, only the tangential principal stress σ_t . σ_t at different positions in Zone II, the inclination angle of the rock formation is different. As it goes deeper into the surrounding rock of the roadway, σ_r increases gradually.

It can be seen from Figure 8 that the stress on the rock mass in Zone II can be decomposed into the bedding force and the force perpendicular to the rock layer. x' is the inclination direction of the rock formation, and y' is the normal direction of the rock formation. The force expressions of the inner rock mass without considering the influence of gravity are:

$$\sigma_{IIx'} = \sigma_{tx'} - \sigma_{rx'} = \sigma_t \cos \beta - \sigma_r \sin \beta \quad (20)$$

$$\sigma_{Ily'} = \sigma_{ry'} + \sigma_{ty'} = \sigma_t \sin \beta + \sigma_r \cos \beta \quad (21)$$

In the formula: β is the angle between the tangential line of the roadway surface and the inclination of the rock formation, and α is the inclination angle of the rock formation. The direction of the force points to the inside of the surrounding rock of the roadway is positive, which is the pressure; the direction of the force is negative when it points to the outside of the roadway, which is the tension force.

Figure 9 is the force diagram of the rock mass on the roadway surface in zone VII. The stress of the surrounding rock on the surface of the roadway in Zone VII is as follows:

$$\sigma_{VIIx'} = \sigma_{rx'} - \sigma_{tx'} = \sigma_t \cos \beta - \sigma_r \sin \beta \quad (22)$$

$$\sigma_{VIIy'} = -\sigma_{ry'} - \sigma_{ty'} = -\sigma_r \sin \beta - \sigma_t \cos \beta \quad (23)$$

(2) Stress Analysis of Rock Mass in Zones III, V and VI

According to the force of the rock mass in zone III on the roadway surface, the force $\sigma_{IIIy'}$ of the rock mass in zone III on the normal line of the rock formation and the force $\sigma_{IIIx'}$ on the inclination direction of the rock formation are shown in Figure 10:

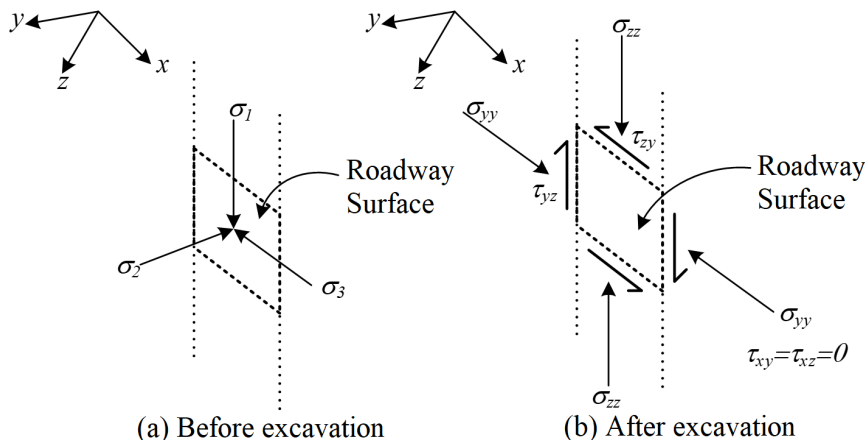


Figure 7. Change of force on the surface of surrounding rock of roadway

$$\sigma_{IIIy'} = \sigma_{ty'} - \sigma_{ry'} = \sigma_t \cos \alpha - \sigma_r \sin \alpha \quad (24)$$

$$\sigma_{IIIx'} = -\sigma_{rx'} - \sigma_{tx'} = -\sigma_r \cos \alpha - \sigma_t \sin \alpha \quad (25)$$

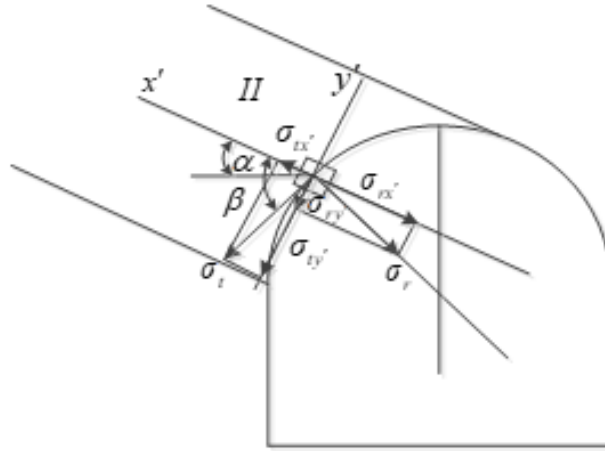


Figure 8. The force diagram of the rock mass in the II area

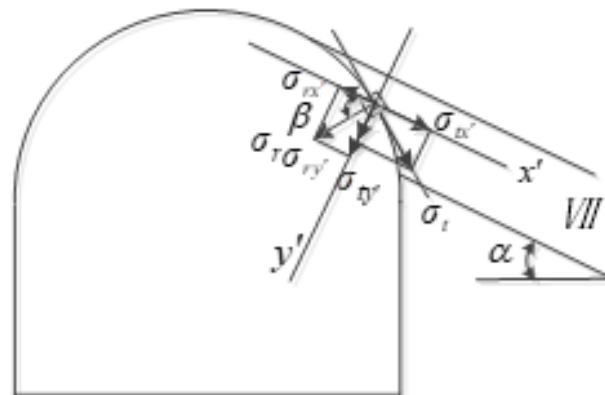


Figure 9. Force diagram of rock mass in area VII

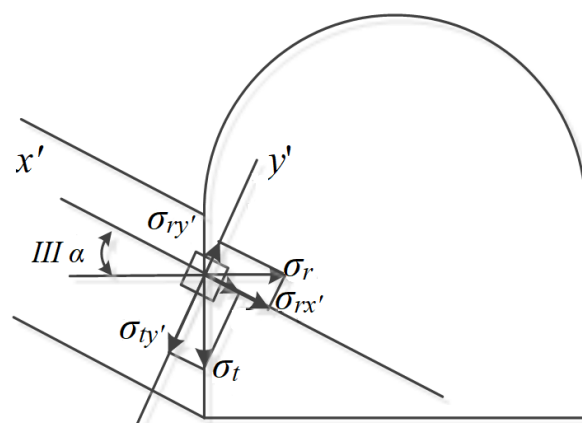


Figure 10. Force diagram of rock mass in zone IIIC

Since the included angle between the rock mass and the roadway surface in Zone III is equal, that is, the stress and magnitude of the rock mass are the same, so the deformation of the rock mass between different rock layers is the same, and there is no interlayer sliding between different rock layers. According to formulas 24 and 25, since σ_r on

the surface of the roadway is zero, $\sigma_{III\ y'}$ is the downward pressure along the normal direction of the rock formation, and $\sigma_{III\ x'}$ is the resultant force of σ_r and σ_t both pointing to the center of the roadway. Therefore, the state of stress of rock in zone III of the roadway is a state of “both tension and compression”. The rock mass beam in the area is prone to tensile failure.

Figure 11 shows the stress analysis of the rock strata in Zone V and Zone VI; Figure 12 shows the mechanical analysis of the rock mass in Zone VI and Zone VII.

It can be seen from Figure 11 that the normal force $\sigma_{V\ y'}$ and bedding force $\sigma_{V\ x'}$ of the rock mass in zone V are:

$$\sigma_{V\ y'} = \sigma_{ry'} + \sigma_{ty'} = \sigma_t \sin \alpha + \sigma_r \cos \alpha \quad (26)$$

$$\sigma_{V\ x'} = \sigma_{tx'} - \sigma_{rx'} = \sigma_t \cos \alpha - \sigma_r \sin \alpha \quad (27)$$

It can be seen from Figure 12 that the normal force $\sigma_{VI\ y'}$ and bedding force $\sigma_{VI\ x'}$ of the rock mass in Zone VI and Zone VII are:

$$\sigma_{VI\ y'} = -\sigma_{ry'} - \sigma_{ty'} = -\sigma_t \cos \alpha - \sigma_r \sin \alpha \quad (28)$$

$$\sigma_{VI\ x'} = \sigma_{tx'} - \sigma_{rx'} = \sigma_t \sin \alpha - \sigma_r \cos \alpha \quad (29)$$

In the rock mass in zone V and zone VI of the roadway, in the normal direction of the rock formation, the stress components in the tangential and radial directions of the roadway are in the same direction. The stress components in the tangential and radial directions are opposite to each other in the bedding direction of the rock formation. The stress state of the rock mass in zone V is represented by the tensile force along the normal direction of the rock formation and the bedding pressure on the rock formation inclination. Under this stress state, the rock mass is prone to bending deformation.

Eqs. (28) and (29) show that, after decomposing the stress of the rock mass and rock strata in zones III, V, VI and VII of the surrounding rock along the normal direction of the rock stratum and along the bedding direction, when the dip angle of the rock stratum is constant, the size of the decomposition force is different. Therefore, assuming that a and b remain unchanged, a schematic diagram of the variation curve of the rock mass stress component with the dip angle of the rock formation in these three regions can be drawn.

Figure 13 shows that the stress of the rock mass in Zone III shows that along with the increase of the dip angle of the rock layer, the tensile force in the direction of the rock layer inclination gradually increases, and the shear stress in the normal direction of the rock layer gradually decreases. The rock mass in the area mainly exhibits tensile failure.

The stress situation of the rock mass in the V area shows that with the increase of the dip angle of the rock layer, the bedding pressure in the direction of the rock layer inclination gradually decreases, the shear stress in the normal direction of the rock layer gradually increases, and the rock mass occurs shear failure.

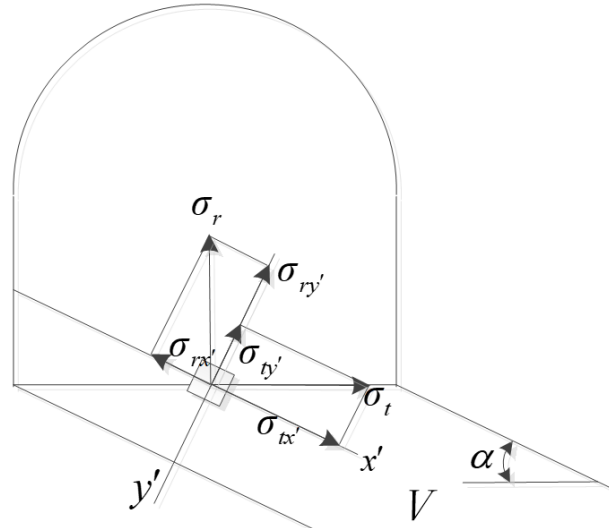


Figure 11. Force diagram of rock mass in area V

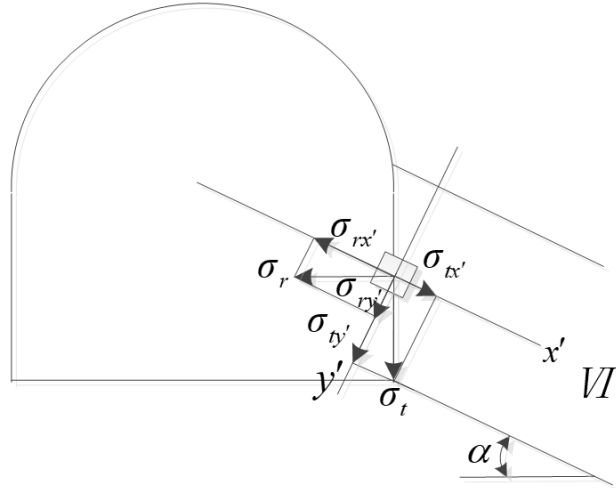


Figure 12. Force diagram of rock mass in area VI and VII

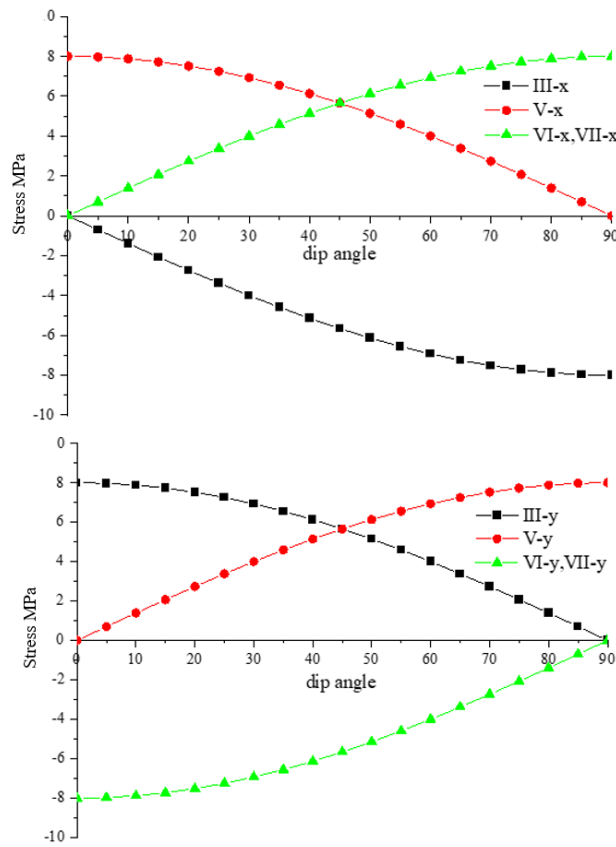


Figure 13. Schematic diagram of the relationship between stress components and rock formation dip

The stress of the rock mass in zone VI shows that with the increase of the dip angle of the rock layer, the bedding pressure in the direction of the rock layer inclination gradually increases, the shear force in the normal direction of the rock layer gradually decreases, and the rock mass suffers pressure failure.

It can be found from the figure that $\sigma_{high-y'}$ and $\sigma_{low-y'}$ decrease continuously with the increase of the dip angle of the rock formation, that is, the interlayer pressure decreases continuously with the increase of the dip angle of the rock formation; $\sigma_{high-x'}$ and $\sigma_{low-x'}$ increase with the increase of the dip angle of the rock formation, that is, the bedding pressure increases with the increase of the dip angle of the rock formation. When the formation dip angle α increases to 90° , $\sigma_{high-x'}$ and $\sigma_{low-x'}$ are equal to the tangential pressure on the roadway surface, and $\sigma_{high-y'}$ and $\sigma_{low-y'}$ become radial pressure and equal to zero.

Based on the above analysis, there are differences in the force form of the free-standing rock mass in the high

and low sides of the roadway. The force form of the high side free-standing rock mass is the combined effect of the pressure perpendicular to the rock formation and the pulling force along the rock formation downwards to the direction of the roadway. The rock mass is prone to tensile failure under this "both compression and tension" force. In the roadway bottom side, the rock mass is subjected to the combined action of the pressure perpendicular to the rock formation and the pulling force along the rock layer down to the direction of the surrounding rock of the roadway. This results in the asymmetry of the two sides deformation in the sloped rock roadway.

3 Slip Danger Identification of Inclined Rock Strata Roadway Surrounding Rock Subareas

The interlayer slip model in the surrounding rock area of the roadway is judged by the slip angle (ω) theory based on the sliding trend judgment of the thin layered surrounding rock of the roadway proposed by Goodman in 1989.

In Figure 14, ω is the angle between the external force and the normal line of the rock joint plane. The slip force on the joint surface between rock formations is $F \sin \omega$. The anti-slip force of the joint surface is $F \cos \alpha \tan \phi$. If interlayer slip and dislocation occur in the surrounding rock of the roadway, Eq. (30) is established, where, ϕ is the internal friction angle of the rock joint plane.

$$F \sin \omega > F \cos \alpha \tan \phi \quad (30)$$

Simplifying Eq. (31) yields:

$$F \tan \omega > F \tan \phi \Rightarrow \tan \omega > \tan \phi \quad (31)$$

That is: $\omega > \phi$. When the included angle (slip angle) between the external force and the normal direction of the rock formation is greater than the friction angle in the joint plane, the layered surrounding rock of the roadway tends to slip between layers.

For the rock mass in Zone III, Zone V and Zone VI, the direction of surface force of the roadway in Zone III and Zone VI and the angle between the normal line of the rock formation are the same but different from Zone V. Suppose the inclination angle of the rock formation is α , because the force on the roadway surface is parallel to the roadway surface, so there is a relationship diagram between the tangential force of the surrounding rock and the joint surface of the rock formation in the II, III, VI and V areas.

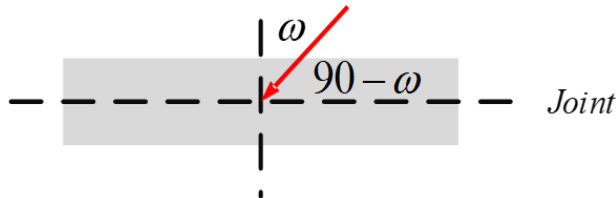


Figure 14. Force model of joint surface

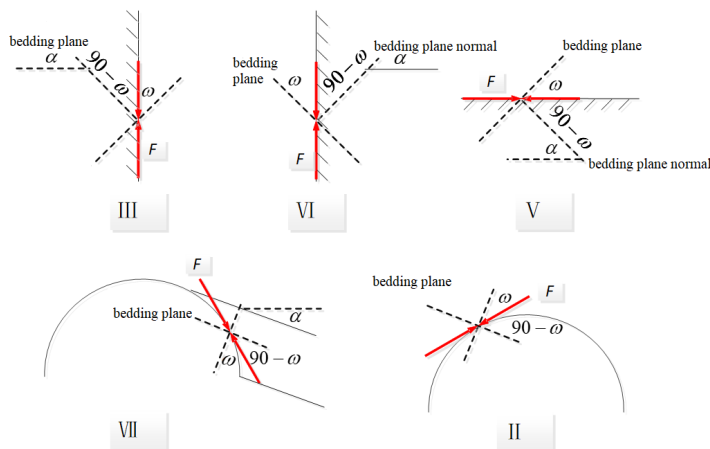


Figure 15. Schematic diagram of slip direction in different partitions

It can be seen from Figure 15 that the slip angle of the rock mass and the dip angle of the rock formation are the same for the roadway surface in Zone III and Zone VI, namely: $\omega = \alpha$; The rock mass in zone V has a slip angle:

$\omega = 90 - \alpha$; The slip angle of zone II and zone VII is the largest at the tangent between the rock formation and the roadway roof. Therefore, when the dip angle α of the rock formation is less than 45° , the slip angle of the rock mass in Zones III and VI is smaller than that in Zone V. Under the same conditions of friction angle and stress in the joint plane, the sliding trend of rock mass in V zone is more obvious than that of zone III and VI. Based on this, it can be determined that the rock mass in the V zone appears to slip earlier than the rock mass in the III and VI zones when the stress increases. From this, the sequence relationship of interlayer slip in surrounding rock of layered inclined roadway can be obtained: Zone II, Zone VII>Zone V>Zone I, Zone IV>Zone VI, Zone III. When the dip angle of the rock formation is greater than 45° , Zone II, Zone VII>Zone VI, Zone III>Zone I, Zone IV > Zone V.

4 Conclusion and Discussion

(1) Different partition models of the layered inclined surrounding rock of the roadway show that the bending internal force in the beam of the surrounding rock mass is related to its lengths L and l . The longer its length is, the greater the bending internal force in the rock mass beam, and the easier it is to exceed its ultimate tensile strength, resulting in tensile failure of the rock mass beam.

(2) There are differences in the force form of the surrounding rock in the high and low sides of the roadway. The stress form of the high-side free rock mass is the combined effect of the pressure perpendicular to the rock formation and the pulling force along the rock formation downward to the direction of the roadway. Under this “both compression and tension” stress form, the rock mass is prone to tensile failure; In the bottom of the roadway, the rock mass is subjected to the combined action of the pressure perpendicular to the rock formation and the pulling force along the rock formation to the direction of the surrounding rock of the roadway. The form is different from the high gang, and it shows three-way pressure, so the bottom gang of the roadway is not easy to be damaged. This results in the asymmetry of the two-gang deformation in the sloped rock roadway.

(3) The sequence relationship of interlayer slip in the surrounding rock of the layered inclined roadway is: when the dip angle of the rock formation is less than 45° , zone II, zone VII>zone V > zone I, zone IV>zone VI, zone III; when the dip angle of the rock formation is greater than 45° , zone II, zone VII>zone VI, zone III>zone I, zoneIV >zone V.

Funding

This research was funded by the National Natural Science Foundation of China, grant number 52074117,51774133.

Data Availability

Data is available on request due to privacy restrictions.

Conflicts of Interest

The authors declare that there are no conflicts of interest regarding the publication of this article.

References

- [1] Y. W. Wang, “China’s coal resource distribution and perspective prediction,” *Coal*, vol. 2007, no. 5, pp. 44–45, 2007. <https://doi.org/10.3969/j.issn.1005-2798.2007.05.019>
- [2] J. Mao and H. Xu, “China’s coal resource distribution and perspective prediction,” *Coal Geol. Explor.*, vol. 1999, no. 03, pp. 2–5, 1999. <https://doi.org/10.3969/j.issn.1001-1986.1999.03.001>
- [3] S. Du, D. Li, and J. Sun, “Stability control and support optimization for a soft-rock roadway in dipping layered strata,” *Geotech Geol Eng.*, vol. 37, no. 3, pp. 2189–2205, 2019. <https://doi.org/10.1007/s10706-018-0753-y>
- [4] Z. G. Tao, C. Zhu, and X. H. Zheng, “Failure mechanisms of soft rock roadways in steeply inclined layered rock formations,” *Geomat Nat Haz Risk.*, vol. 9, no. 1, pp. 1186–1206, 2018. <https://doi.org/10.1080/19475705.2018.1497712>
- [5] Y. H. Zhang, J. Underschultz, L. Langhi, D. Mallants, and J. Strand, “Numerical modelling of coal seam depressurization during coal seam gas production and its effect on the geomechanical stability of faults and coal beds,” *Int J Coal Geol.*, vol. 195, pp. 1–13, 2018. <https://doi.org/10.1016/j.coal.2018.05.008>
- [6] A. T. Zhou, J. Y. Hu, W. L. Gong, K. Wang, N. Deng, and J. C. Wu, “The instability criticality and safety factor of coal-gas outburst induced by shear failure based on limit analysis,” *Fuel.*, vol. 303, 2021. <https://doi.org/10.1016/J.FUEL.2021.121245>
- [7] Y. X. Yu, X. Hong, and F. F. Chen, “Study on load transmission mechanism and limit equilibrium zone of coal-wall in extraction opening,” *J. China Coal Soc.*, vol. 37, no. 10, pp. 1630–1636, 2012. <https://doi.org/10.13225/j.cnki.jccs.2012.10.017>

- [8] H. S. Tu, S. H. Tu, X. G. Zhang, Z. X. Li, and S. Jia, “Technology of back stoping from level floors in gateway and pillar mining areas of extra-thick seams,” *Int J Min Sci Techno.*, vol. 24, pp. 143–149, 2014. <https://doi.org/10.1016/j.ijmst.2014.01.001>
- [9] C. Zhu, Y. Yuan, Z. S. Chen, C. G. Meng, and S. G. Wang, “Study of the stability control of rock surrounding longwall recovery roadways in shallow seams,” *Shock Vib.*, 2020. <https://doi.org/10.1155/2020/2962819>
- [10] S. Li, W. Wang, and C. Pan, “Numerical analysis on support structure of rock around deep roadway,” *Chin. J. Geotech. Eng.*, vol. 2006, no. 03, pp. 377–381, 2006. <https://doi.org/10.3321/j.issn:1000-4548.2006.03.018>
- [11] H. Wang, C. Jiang, P. Q. Zheng, N. Li, and Y. B. Zhan, “Deformation and failure mechanism of surrounding rocks in crossed-roadway and its support strategy,” *Eng. Fail. Anal.*, vol. 116, 2020. <https://doi.org/10.1016/j.engfailanal.2020.104743>
- [12] S. Li, C. Pan, and W. Wang, “Analysis of plastic region of sidewalls in coal drifts reinforced by association of rock bolt and grouting,” *J. Hunan Univ. Sci. Technol.*, vol. 2007, no. 02, pp. 5–8, 2007. <https://doi.org/10.1325/j.cnki.jccs.2011.10.014>
- [13] Y. L. Tan, H. L. Wang, D. Y. Fan, X. S. Liu, and X. Wang, “Stability analysis and determination of large-section multi-chamber group in deep coal mine,” *Geomech. Geophys. Geo.*, vol. 8, no. 01, 2021. <https://doi.org/10.1007/s40948-021-00312-y>
- [14] X. J. Zhu, G. L. Guo, H. Liu, X. N. Peng, and X. Y. Yang, “Research on the stability evaluation model of composite support pillar in backfill-strip mining,” *Math. Probl. Eng.*, pp. 1–11, 2020. <https://doi.org/10.1155/2020/3138258>
- [15] M. Satar, “Prediction of tailgate stability in mechanized longwall mines using an improved support vector regression model,” *Arab J. Geosci.*, vol. 14, no. 03, 2021. <https://doi.org/10.1007/s12517-021-06598-2>
- [16] W. Wang and C. Hou, “Mechanism analysis of top coal and caving roadway deformation in steep seam,” *Chin. J. Geotech. Eng.*, vol. 2001, no. 05, pp. 623–626, 2001. <https://doi.org/10.13225/j.cnki.jccs.2000.01.009>
- [17] X. H. Wu, B. B. Li, and C. H. Ren, “An original coupled damage–permeability model based on the elasto-plastic mechanics in coal,” *Rock Mech Rock Eng.*, vol. 55, no. 04, pp. 1–18, 2022. <https://doi.org/10.1007/s00603-022-02771-5>
- [18] X. Y. Xu, Y. M. Li, and J. Lu, “The use of surrounding rock loosening circle theory combined with elastic-plastic mechanics calculation method and depth learning in roadway support,” *Plos One.*, vol. 15, no. 07, pp. 1–13, 2020. <https://doi.org/10.1371/journal.pone.0234071>
- [19] D. Yun, C. Wang, P. Su, P. Xie, Y. Zhou, Y. Xin, H. Liu, and L. Chen, “Support technology of mining gateway in high inclined seam with soft top coal,” *Coal Sci. Technol.*, vol. 38, no. 10, pp. 13–16, 2010. <https://doi.org/10.13199/j.cst.2010.10.20.yundf.020>
- [20] D. Yun, Y. Xin, H. Ji, C. Wang, P. Su, H. Liu, and L. Chen, “Roof monitor and supports design of pitched “three soft” prominent coal seam,” *J. Xi’An Univ. Sci. Technol.*, vol. 30, no. 03, pp. 260–265, 2010. <https://doi.org/10.13800/j.cnki.xakjxxb.2010.03.005>
- [21] X. Gao, Z. K. Ma, and H. Y. Shi, “Energy release induced rockbursts based on butterfly-shaped plastic zones in roadways of coal reservoirs,” *Plos One*, vol. 16, no. 07, 2021. <https://doi.org/10.1371/journal.pone.0255044>
- [22] M. Li, H. T. Wang, D. M. Wang, and Z. L. Shao, “Experimental study on characteristics of surface potential and current induced by stress on coal mine sandstone roof,” *Eng Geol*, vol. 266, 2020. <https://doi.org/10.1016/j.enggeo.2019.105468>
- [23] X. Lai, J. Ma, W. Zhang, Q. Wang, and F. Cui, “Field monitoring of localized deformation characteristics around rock in steep coal seam,” *J. XI’AN Univ. Sci. Technol.*, vol. 32, no. 04, pp. 409–414, 2012, in Chinese. <https://doi.org/10.13800/j.cnki.xakjxxb.2012.04.012>
- [24] M. Wang, D. G. Zheng, S. J. Niu, and W. F. Li, “Large deformation of tunnels in longwall coal mines,” *Environ Earth Sci*, vol. 78, no. 2, p. 45, 2019. <https://doi.org/10.1007/s12665-019-8044-3>
- [25] B. Tang, Z. H. Wang, and H. Cheng, “Experimental study on pipe strength and field performance of pipe jacking tbm in deep-buried coal mines,” *Int J Civ Eng*, vol. 19, no. 11, pp. 1–12, 2021. <https://doi.org/10.1007/s40999-021-00632-w>
- [26] S. H. Tu, Z. X. Li, Z. W. Ye, C. Zhang, and L. Zhang, “The complex function method roadway section design of the soft coal seam,” *Math Probl Eng*, no. 10, 2016. <https://doi.org/10.1155/2016/9291412>
- [27] J. Wang, Z. B. Guo, Y. B. Yan, J. W. Pang, and S. J. Zhao, “Floor heave in the west wing track haulage roadway of the tingnan coal mine: Mechanism and control,” *Int. J. Min. Sci. Technol.*, 2012. <https://doi.org/10.1016/j.ijmst.2012.04.002>
- [28] S. Guo, X. G. Zhu, X. Liu, and H. F. Duan, “A case study of optimization and application of soft-rock roadway support in xiaokang coal mine, china,” *Adv. Civ. Eng.*, 2021. <https://doi.org/10.1155/2021/3731124>
- [29] N. Wang, N. Zhang, H. Lan, and T. Zhang, “Analysis of field surface and underground coordination detection

- to mined-out-area surrounding steep-heavy thickness coal seam," *J. Xi'An Univ. Sci. Technol.*, vol. 33, no. 01, pp. 7–11, 2013. <https://doi.org/10.13800/j.cnki.xakjdxxb.2013.01.014>
- [30] H. B. Chu, G. Q. Li, and Z. J. Liu, "Multi-level support technology and application of deep roadway surrounding rock in the suncun coal mine, china," *Materials*, vol. 15, no. 23, pp. 8665–8665, 2022. <https://doi.org/10.3390/ma15238665>
- [31] J. Li, X. Qiang, N. Ma, R. Zhang, and B. Li, "Formation mechanism and engineering application of the directionality of butterfly leaf in the butterfly plastic zone of roadway rock surrounded," *J. China Coal Soc.*, vol. 46, no. 09, pp. 2838–2852, 2021. <https://doi.org/10.13225/j.cnki.jccs.2021.1150>
- [32] L. Meng, Y. Huang, T. Li, B. Chen, W. Zhang, H. Chen, and H. Li, "An improved classification method of asymmetrical squeezing large deformation of layered soft rock tunnels under high geo-stresses," *Chin. J. Rock Mech. Eng.*, vol. 41, no. 01, pp. 147–156, 2022. <https://doi.org/10.13722/j.cnki.jrme.2021.0613>
- [33] C. L. Liu and G. H. Zhang, "Instability analysis and reinforcement support technology of coal-rock interbed roadway in gaojiazhuang coal mine," *Adv. Civ. Eng.*, 2021. <https://doi.org/10.1155/2021/5542830>
- [34] Q. H. Li, J. K. Li, and J. P. Zhang, "Numerical simulation analysis of new steel sets used for roadway support in coal mines," *Metals*, vol. 9, no. 5, p. 606, 2019. <https://doi.org/10.3390/met9050606>
- [35] S. Hu, "Characteristics and mechanism of deformation and failure of layered surrounding rock mass in deep roadway," *Chin. J. Rock Mech. Eng.*, vol. 34, no. 11, p. 2376, 2015. <https://doi.org/10.13722/j.cnki.jrme.2015.2004>
- [36] H. Tian, W. Chen, X. Tan, Y. Tian, and N. Zhang, "Investigating polymeric foam materials as compressible layer for tunnelling in squeezing ground conditions," *Tunn. Undergr. Space Technol.*, vol. 122, p. 104391, 2022. <https://doi.org/10.1016/j.tust.2022.104391>
- [37] H. Wu, X. Wang, W. Wang *et al.*, "Deformation characteristics and mechanism of deep subsize coal pillar of the tilted stratum," *Energy Sci. Eng.*, vol. 8, no. 2, pp. 544–561, 2020. <https://doi.org/10.1002/ese3.546>
- [38] H. Wu, Q. Jia, W. Wang *et al.*, "Experimental test on nonuniform deformation in the tilted strata of a deep coal mine," *Sustainability*, vol. 13, 2021. <https://doi.org/10.3390/su132313280>
- [39] Q. Jia, H. Wu, T. Ling *et al.*, "Study on the stress variation law of inclined surrounding rock roadway under the influence of mining," *Minerals*, vol. 12, 2022. <https://doi.org/10.3390/min12050499>
- [40] X. Li, X. Zhou, B. Hong *et al.*, "Experimental and analytical study on longitudinal bending behavior of shield tunnel subjected to longitudinal axial forces," *Tunn. Undergr. Space Technol.*, vol. 86, pp. 128–137, 2019. <https://doi.org/10.1016/j.tust.2019.01.011>
- [41] X. Wu, Y. Jiang, Z. Guan *et al.*, "Influence of confining pressure-dependent young's modulus on the convergence of underground excavation," *Tunn. Undergr. Space Technol.*, vol. 83, pp. 135–144, 2019. <https://doi.org/10.1016/j.tust.2018.09.030>
- [42] Z. Zhang, M. Zhang, Y. Jiang, Q. Bai, and Q. Zhao, "Analytical prediction for ground movements and liner internal forces induced by shallow tunnels considering non-uniform convergence pattern and ground-liner interaction mechanism," *Soils Found.*, vol. 57, no. 2, pp. 211–226, 2017. <https://doi.org/10.1016/j.sandf.2017.03.004>
- [43] W. Gao, *Rock Mechanics*. Peking University Press, 2010.
- [44] Z. Chen, *Stability Analysis of Rock Slope*. China Water Resources and Hydropower Press, 2005.
- [45] G. G. Zhao, C. Y. Liu, S. M. Kao, X. B. Zhang, and X. Cheng, "Stress and load-bearing structure analysis of the surrounding rock in a soft broken roadway," *Arab J Geosci*, vol. 13, no. 21, 2020. <https://doi.org/10.1007/s12517-020-06126-8>
- [46] H. Liu, *Mechanics of Materials*. Higher Education Press, 2011.
- [47] R. E. Goodman, *Introduction to Rock Mechanics*. John Wiley & Sons, 1989.